Preprint Title	The Control on Morphology and Crystallinity of CNT in Flame Synthesis with One-Dimensional Reaction Zone
Authors	Muhammad Hilmi Ibrahim, Norikhwan Hamzah, Mohd Fairus Mohd Yasin, Mohd Zamri Mohd Yusop and Ni Luh Wulan Septiani
Publication Date	20 Jan. 2023
Article Type	Full Research Paper
ORCID® iDs	Muhammad Hilmi Ibrahim - https://orcid.org/0000-0003-3772-4822

The Control on Morphology and Crystallinity of CNT in Flame Synthesis with One-Dimensional Reaction Zone

Muhammad Hilmi Ibrahim[‡1,2], Norikhwan Hamzah[‡1,2], Mohd Fairus Mohd Yasin[*1,2], Mohd Zamri Mohd Yusop[‡3], Ni Luh Wulan Septiani[4]

Address: [1]Department of Thermo-Fluids, School of Mechanical Engineering, Faculty of Engineering, Universiti Teknologi Malaysia, 81310 Johor Bahru, Malaysia, [2]High Speed Reacting Flow Laboratory (HiREF), Universiti Teknologi Malaysia, [3]Advanced Membrane Technology Research Center, Universiti Teknologi Malaysia, [4]National Research and Innovation Agency, Indonesia

Email: mohdfairus@utm.my

* Corresponding author

‡ Equal contributors

Abstract

The growth of carbon nanotubes (CNT) in flame requires imperative conditions that are difficult to achieve in a highly heterogeneous environment. Therefore, the analysis of the properties of the reaction zone within the flame is critical for the optimal growth of CNT. In the present study, a comprehensive comparison between the CNT synthesis using methane diffusion flame and that of premixed flame is conducted regarding the

morphology and crystallinity of the as-grown nanotubes. The premixed burner configuration created a flame that isstabilized across axisymmetric stagnation flow through sintered metal, making the flame one-dimensional in nature as opposed to the co-flow configuration of diffusion flame. The significant difference in temperature distribution between the two flames causes the difference in the characteristic pattern of the growth products. In diffusion flame, the growth is limited to specific regions at certain height-above-burners (HAB) with suitable thermochemical conditions. The identified growth regions at different HAB showed similar temperature distribution that produces CNT of similar characteristics. In contrast with premixed flame, the growth of CNT dictates by only the HAB due to relatively uniform temperature distribution along the radial directions but significantly different in the vertical direction.

Keywords

Carbon nanotubes; flame synthesis; one-dimensional flame; morphology; crystallinity; synthesis control

Introduction

Carbon nanotubes have been the research topic for a few decades since the discovery by Iijima [1] in 1991. The morphology of the CNT structure exhibits remarkable mechanical, electrical, and thermal properties. The studies of CNT synthesis using different methods have been reported to produce nanotubes that exhibit varying properties in terms of morphology, size, types, and functionalization [2]. Controlling nanotube properties is essential for implementing the material into various applications.

In a recent study on the production of CNT-based conductive textiles, the fabrication of conductive wool requires the utilization of multi-walled CNT (MWCNT) with a carboxylated functionalization [3].

On the other hand, the aerospace industry utilizes CNT with high thermal, chemical, mechanical, and electrical performance as nanocomposite additive to overcome problems in aircraft coatings, such as corrosion, ice accretion, lightning strike, and erosion. Overall, CNT/epoxy nanocomposite that exhibits superior mechanical properties is preferred to push the performance limit of the end product [4]. Scarselli et al. [5] synthesized CNT with a three-dimensional network using a sulphur enhancer and created a porous product capable of adsorbing oils. Furthermore, the CNT networks also have a high potential to be utilized in photon-energy conversion devices due to the excellent photo response in the incident and near UV light. Hence, the ability to control nanomaterial morphology and functionalization during the synthesis process will open vast opportunities to satisfy the needs of various specific applications is desired. To date, many researchers have shown promising results on the synthesis control of CNT that produce bespoke CNT morphology and properties through the conventional furnace-based method.

The progress in development of CNT synthesis process has been achieved mostly using the chemical vapor deposition (CVD) method. Various studies on the growth control in CVD synthesis conclude that the simple manipulation of independent parameters such as fuel selection, synthesis temperature, vapor pressure, and catalyst are the governing parameter in CNT growth [6]; all can be manipulated for the synthesis control. For most studies, CVD is preferred due to the high degree of control and ability to synthesize at

relatively low temperatures. However, the CVD process requires a high energy consumption for CNT growth, leading to an increased production cost and thus making the price of high-quality CNT too expensive to be applied in various applications. Alternatively, the similar growth mechanism of CNT using a least common method, flame synthesis, is explored. In flame synthesis, the correct selection of catalyst is the governing parameter that produces CNT similar to that made in CVD with some degree of control in an economical production process [7].

Hamzah et al. [8] discussed the CNT morphology and growth control in flame synthesis over many parameters such as fuel, catalyst, temperature, and diluent. However, the heterogeneous gas properties from combustion involve high-temperature gradient and wide chemical species distribution within the flame environment. The interrelated process of heat generation and carbon supply requires optimum parametric control to achieve a stable growth condition. However, achieving independent parametric control in flame synthesis is a challenging task. In diffusion flame, specific locations within the flame are imperative and conducive for CNT growth depending on the HAB, local distance from the flame front, and flame composition [9].

In another study, a premixed flat flame was utilized by Zhang et al. [10] to synthesize single-walled CNT (SWCNT) in rich hydrogen/air combustion with a ferrocene catalyst. The temperature profile is estimated to be relatively uniform across HAB up to 10 mm. An increase in CNT yield is observed at a high mass flux of hydrogen/air mixture at fixed equivalence ratio, resulting in more heat release, higher temperature, and an increasing I_G/I_D ratio of up to 10 times. A similar approach in spray pyrolysis CVD by Casanova et al. [11] utilizing ferrocene catalyst with cyclohexanol as carbon source, however, shows that

a variety of growth temperatures produces CNT with similar crystallinity. Although, in a study by Chong et al. [12], the combustion of propane premixed flame at varying equivalence ratios yielded similar effects on CNT growth, whereas the Transmission Electron Microscopy (TEM) analysis shows the morphology of MWCNT similar to that of CVD. Raman spectroscopy shows I_G/I_D ratios are constant for all runs, and Thermogravimetric Analysis (TGA) results show almost equal CNT oxidation temperature, indicating similar purity. The constant crystallinity from I_D/I_G ratio is also shown in another study by Hamzah et al. [13] utilizing methane diffusion flame sampled at a different air flow rate.

The present study will utilize the usage of methane combustion in diffusion and premixed flat flame in synthesizing CNT from nickel wire. The morphology and crystallinity effects on the grown CNT will be compared and analyzed to better understand the governing parameters that can be manipulated in synthesis control.

Results and Discussion

Flame characterization and temperature

The flames employed in the present study are characterized based on the flame shape, spatial distribution of the reaction zone, and temperature distribution. Figure 1(a)-(b) compare the line-of-sight images of the diffusion flame and the flat premixed flame burned at rich combustion of 1.16 and 1.8 equivalence ratio, respectively, where the equivalence ratio is calculated based on the inlet conditions. The diffusion flame in formed a bright yellow color due to the soot formation with a height of 55 mm. Figure 1(c) shows that in diffusion flame, the temperature increases at high HAB in radial locations near the flame

sheet. As expected, the temperature is low near the burner due to burner heat loss, while the heat generation within the reaction zone of the blue flame sheet increases the local temperature. For CNT growth, it is reported in many studies that the ideal temperature are in between 750 ^{o}C and 950 ^{o}C [14], [15]. Hence, for diffusion flame, the CNT growth region are located at higher HAB and near the flame center where the temperature is within the growth temperature range [13].

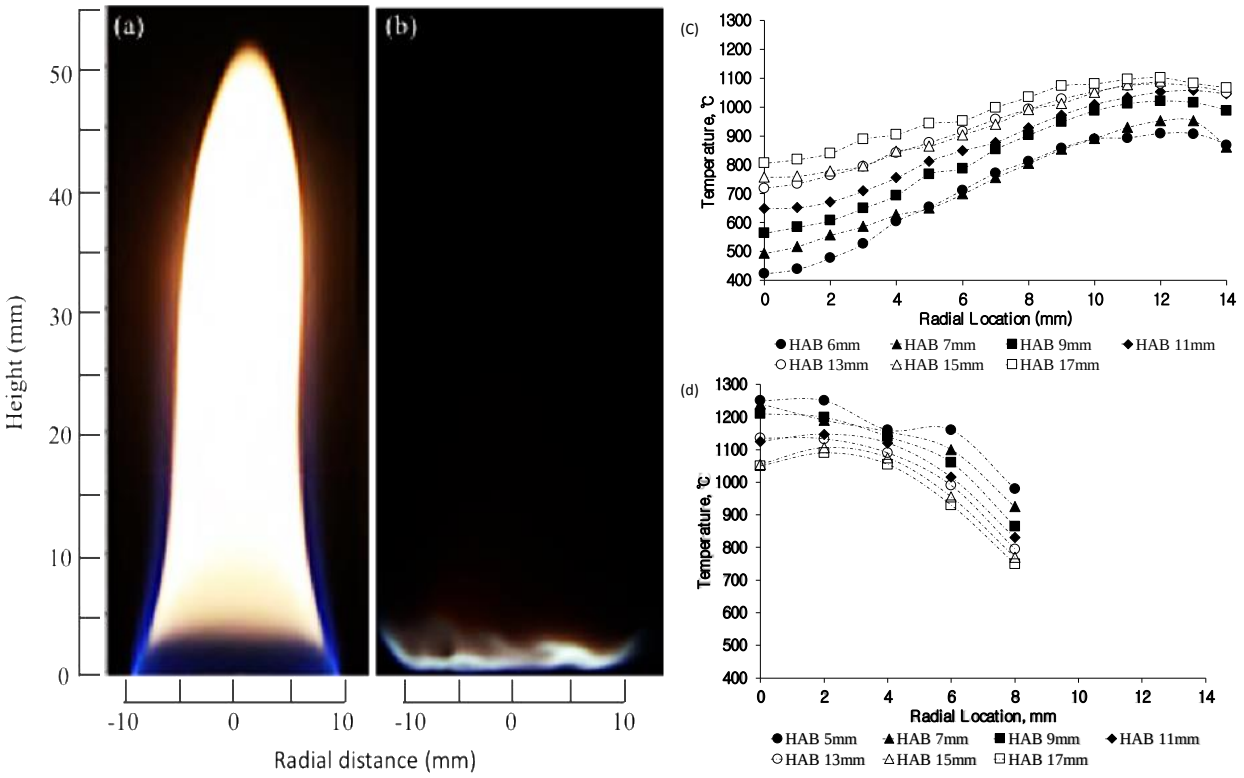

Figure 1: Line-of-sight images of standing flame and temperature distribution of (a)&(C) diffusion flame and (b)&(d) premixed flame. Fig. 1 (a) was used with permission of Elsevier Science & Technology Journals, from [9], ("Effect of fuel and oxygen concentration toward catalyst encapsulation in water-assisted flame synthesis of carbon nanotubes", N. Hamzah et al., Combustion and Flame, vol. 220, © 2020); permission

In the premixed flame setup, the utilization of sintered metal allows for a uniform gas flow distribution producing a flat flame shape, as shown in Figure 1(b). The one-dimensional flame with a uniform blue color intensity suggests uniform temperature distribution across the radial location. The shield at the outer annulus provides encapsulation of the primary flame and avoids the entrainment of ambient air into the reactant stream that may lead to the formation of a secondary diffusion flame. Figure 1(d) shows temperature uniformity at all HAB up to 8 mm radial distance from the flame center, which is not observed in a diffusion flame. The maximum temperature is at 0-2mm from the centerline of the lowest HAB 5 mm. However, the temperature drop is observed at the far-field region away from the flame center line. The difference in temperature at the flame center and flame sheet is due to the effect of cold shield gas flow at the outer annulus. The stated trend is also observed at all HAB though the temperature at all locations is still within the imperative condition for CNT growth. The height of the flame only reaches up to 5 mm, hence the term “flat.” The flame heights are varied according to the equivalence ratio and oxygen concentration of the flame [16]. A separate test shows that the flame loses its one-dimensional characteristics at an O_2 concentration below 34%. A previous study shows that the consistency of the one-dimensional flame is vital to achieve the uniformity of flame characteristics in the radial direction [17], which is useful for consistent CNT growth along the metal wire in the present study.

CNT Growth

In general, the growth of CNT via nickel wire starts from a process of surface breakup in a carbon-rich high-temperature environment that forms a rough surface covered with nanoparticles. The carbide layer formed on the wire will induce the localized stresses on the surface region due to the lattice mismatch and the break up along the grain boundaries creating particles of various size and shape [13]. According to the widely accepted Vapor-Liquid-Solid mechanism, the growth of CNT occurs in three steps, namely, reduction of nickel particles into a molten state, adsorption of carbon atoms onto the surface of the metal nickel, and finally, diffusion and deposition of the precipitated carbon that form tubular materials by curling of graphene sheet on the surface [18], [19]. In flame synthesis, the rapid heating rate causes the catalytic activation and nucleation to occur almost instantaneously by the arrangement of carbon atoms on the catalyst nanoparticle's surface, leading to cap formation and lift-off.

Figure 2(b) and (d) show FESEM images at 50K magnification of the grown CNT on nickel wire diffusion and premixed flame, respectively. The synthesized CNT formed long curly and bent tubes is grown in random orientation with the presence of the catalyst particles attached to the tubes, as observed in both images. Generally, CNT will follow a particular atomic arrangement and grow out vertically in the substrate's normal direction [20] because the CNT containing catalyst particles grows heading outwards. The said growth model is similar to the mechanism proposed by Baker et al. [21]–[23]. At elevated temperatures, the catalytic particles are formed on the substrate's surface before the hydrocarbon molecules that experience cracking with the flame diffused to the catalyst's surface, where carbon atoms absorbed by the catalyst are deposited by diffusion for

continuous stacking of nanotubes. The weak interaction force between the catalyst particle and the substrate lifts the particles as the nanotubes grow, forming CNTs with catalyst particles on the tip. CNTs are formed with catalyst particles at the bottom of the catalyst-substrate interaction force is more substantial [23]. Nevertheless, the rapid growth of CNT was observed from the active catalytic activities reaction within the flame environment.

Due to the coupled energy and mass transfer phenomenon, temperature and gas-phase chemistry evolution co-occur inside the flame [24], thus enabling the particle formation and CNT growth to occur almost instantaneously. The rapid particle formation from the surface breakup produces a heterogenous particle size. Consequently, particle bundles can be observed, revealing the particles' agglomeration and sintering during the flame's high-temperature growth. The point-based EDX analysis in Table 1 shows a high level of nickel. A previous study shows that the formation of nickel particles of 5 nm and above can be reactive towards CH4, which is favorable for CNT growth [12].

Table 1: Average Elemental composition of CNT on nickel wire by EDX

Element	C	O	Ni
Content/wt%	83.4	4.75	11.85
Variance,σ	2.50	0.85	2.13

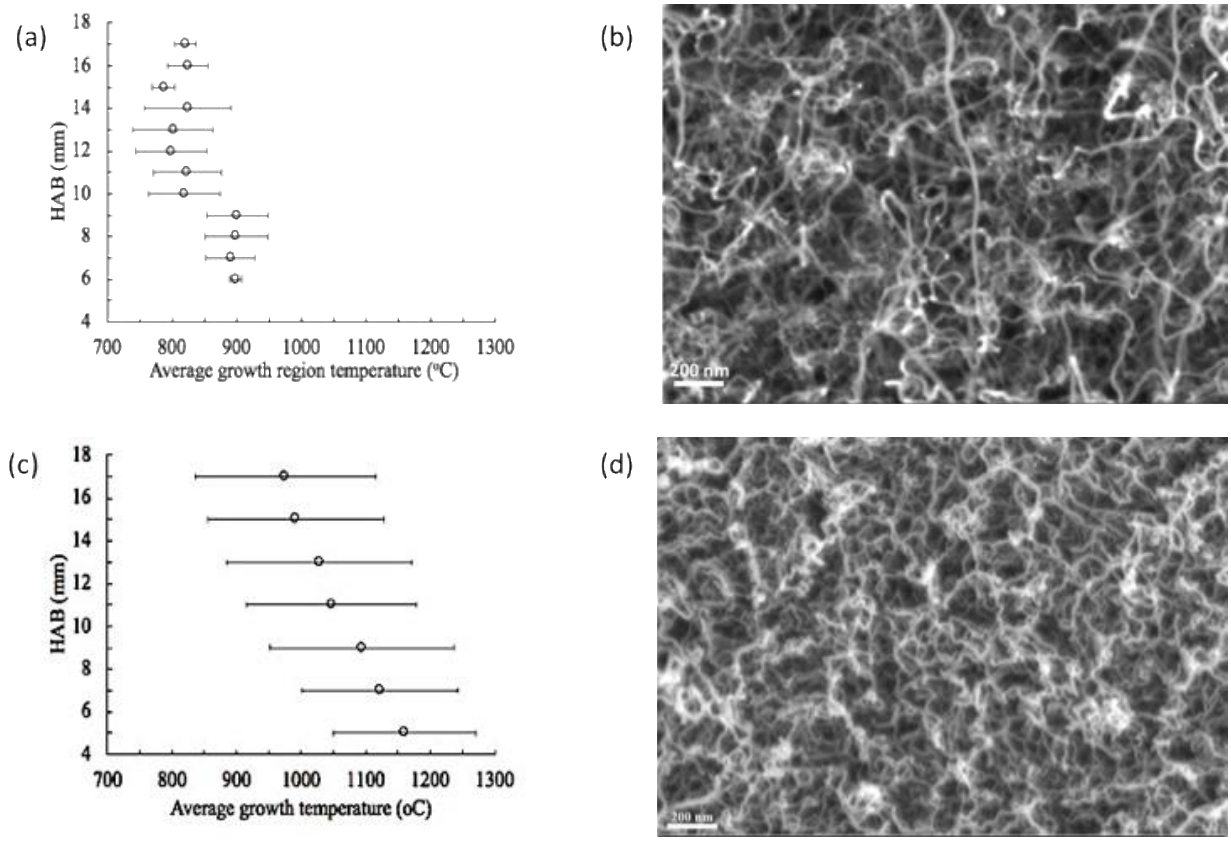

Figure 2: Average growth region temperature and the corresponding FESEM images of of CNT in nickel wire synthesized by (a)&(b) Diffusion flame and (c)&(d) premixed flame.

The average growth temperature for both diffusion and the premixed flame is shown in Figure 2 (a) and (c), respectively. For diffusion flame, CNT growth extends from the near vicinity of the flame sheet towards the flame centerline, within the fuel stream where an abundance of carbon sources flows. The growth regions stop growing when the local temperature falls below the minimum growth temperature. The growth temperature is measured at the growth region. As observed, there is a gap of average temperature around 100 ^{o}C for growth regions below 9 mm and above 10 mm. The temperature difference is caused by the location of the growth region, as discussed above. The temperature of the high HAB region (above 10 mm) is lower due to the relatively faster

carbon inception process due to the abundance of carbon sources and adequate temperature, specifically inside the fuel stream flow. Contrarily, the low HAB region has no growth inside the fuel stream (below 9 mm) due to lower temperatures. Instead, growth occurs inside the oxidizer stream flow at the flame sheet, although the growth region shrinks due to a lack of carbon sources.

In premixed flame, the temperature across the radial location is relatively uniform and within the ideal conditions. Thus, CNT growth can occur at all regions radially. The temperature uniformity across radial locations is expected to produce less heterogeneous particle size during particle formation. The average growth temperature in premixed flame is then measured for all regions. Interestingly, there is a significant difference of 200 ^{o}C in temperature distribution at lower and higher HAB. The lowest HAB temperature shows the highest temperature reading and linearly decreases at higher HABs. The temperature differences are expected to produce different particle size distributions. The CNT diameter, which often correlates to particle size, shows a similar trend, as discussed in the next section.

CNT Characterization

The diameter of the synthesized CNT is measured using an image post-processing software, Digimizer^{TM}, with 200-300 data per sample to produce the size histogram. Figures 3(a) and (b) shows the CNT diameter distribution for growth in diffusion and premixed flame, respectively. In diffusion flame synthesis, the CNT diameter distribution at every sampled HAB shows no significant difference, with an average of around 16.3 nm, ranging from 10-35 nm. The high skewness of the standard deviation indicates a diameter variation due to heterogeneous particle size formation. Nevertheless, the

consistency in CNT diameter at all HAB shows the stable growth region location to produce CNT of the same morphology viably. The identified regions will likely share a common temperature-gas phase distribution relation attractive for CNT inception and growth. Although the rate of inception could be varied, the effects do not reflect on the size of the CNT formed.

Figure 3(b) shows a linear trend in the CNT diameter distribution at different HAB. Smaller average CNT diameter was synthesized at higher HAB in premixed 1D flame with a 10 nm maximum change in diameter. At lower HAB, the big CNT diameter with high skewness in standard deviation suggests various sizes of particles formed during the growth process, possibly due to the high-temperature region at lower HAB. Generally, the nanoparticle size is prepared by several factors, including solution concentration, deposition method, quantity, and annealing [25]. At higher temperatures near lower HAB, the particle can combine, sinter, and increase in size either due to Ostwald's ripening or particle migration and coalesce phenomena [26]. The agglomeration happens because of the high-temperature process that creates a condition similar to annealing. At higher HAB, where the temperature is relatively low, the CNT diameter decreases with smaller skewness in deviation, implying the formation of more uniform particle size.

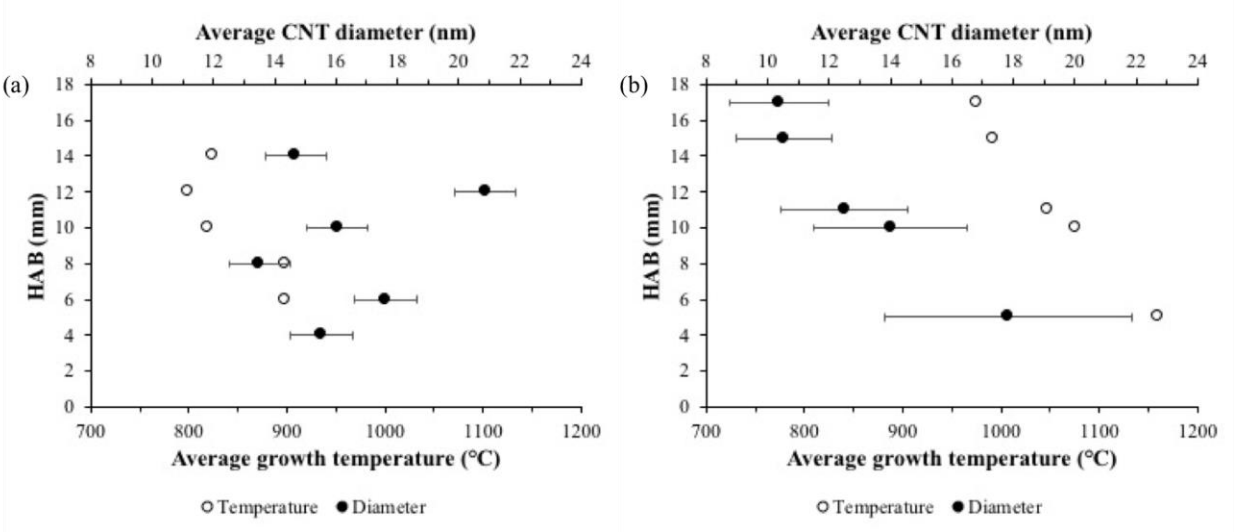

Figure 3: Average CNT diameter distribution with relative temperature for (a) diffusion flame and (b) premixed flame

Figure 4 shows the Raman spectra of the CNTs grown with (a)diffusion flame and (b) premixed flame at highest and lowest HAB. Generally, the formation of an sp2-bonded carbon atom with high degree order and symmetry is often correlated to the characteristics of Raman scattering having G-peaks at around 1550~1600 cm^{-1}. Similarly, the D-peak around 1250~1450 cm^{-1} often correlates to defects and disorder of the sp2 sidewalls, while the G' peak at 2500~2900 cm^{-1} represents the photon-second phonon interaction [27]. The absence of a low-frequency peak <200cm^{-1}, usually assign to A_{1g} symmetry radial breathing mode (RBM), which is the main trait for single-walled CNT (SWCNT) [28], indicates that the products of both syntheses are multi-walled CNT (MWCNT). In addition, the broad asymmetric feature in G-band shows the properties of MWCNT as compared to SWCNT or graphite, which has a double peak and narrow peak, respectively. The D-band (ID) and G-band (IG) intensities show an I_D/I_G ratio of less than

1.00, indicating the presence of high crystallinity and purity of CNT. DiLeo theorizes that purity can be determined from the $I_{G'}/I_{D,}$ where a higher ratio indicates a higher purity [29].

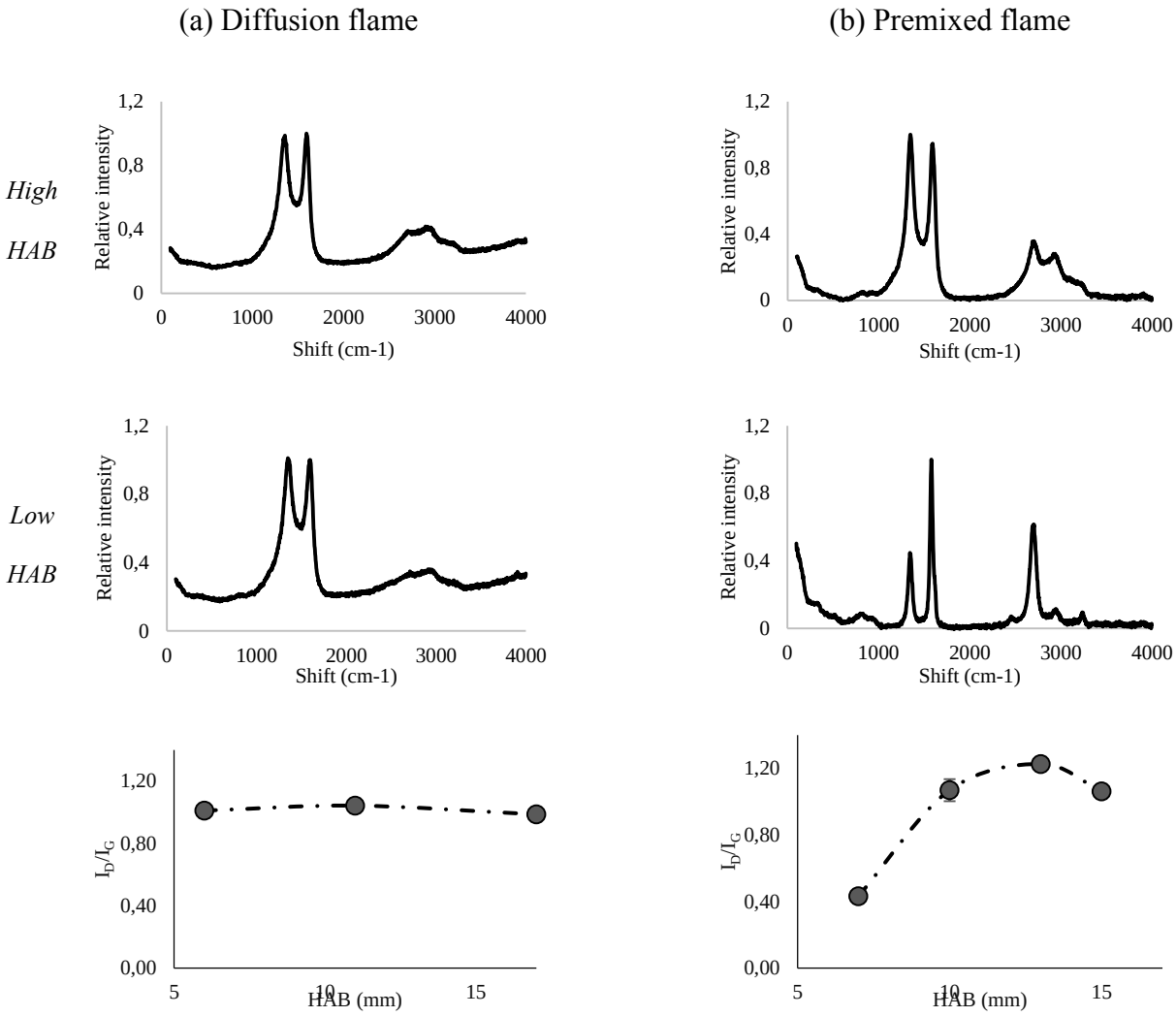

Figure 4: Raman shift of CNT at low, high, and average HAB for (a) diffusion flame and (b) Premixed flame

In diffusion flame, the I_D/I_G at low, middle, and high HAB shows a constant trend within the range of 0.98 to 1.01, indicating consistency in crystallinity. The almost identical shift of CNT at all HAB indicates the uniformity in terms of particle formation and CNT growth, as shown by the diameter distribution. As the identified growth region creates similar

growth conditions, the process at every HAB produces CNT of similar purity and crystallinity.

In the premixed flame, the I_D/I_G ratio increases at higher HAB. As expected, the amount of carbon supply at lower HAB is essentially higher, leading to a higher graphitic band's peak. The increase in D band peaks with lower MWCNT content at higher HAB directly results from the addition of carbonaceous by-products. However, the I_D/I_G ratio seems to settle at around 1.00 at a much higher HAB. Hence, the crystallinity and graphitization of the products are inversely proportional to the diameter, as discussed previously, leaving a trade-off that requires optimization.

Conclusion

The growth of CNT in the diffusion and the premixed flame is extensively studied and compared. Diffusion flame possesses a highly non-uniform temperature distribution which can only grow CNT at a specific location within the flame. Because of the similar condition of these growth regions, the characteristics of the as-grown products are also similar. On the other hand, premixed flame shows a more uniform temperature distribution across the radial direction. The temperature difference is only observed at higher HAB. The products synthesized by the premixed flame are dictated by the condition of the growth location, which only varies by the HAB. Thus, a more uniform parametric difference can be observed and utilized for future optimization.

Experimental

Catalyst preparation

Nickel wire is used where the catalyst, namely nickel nanoparticles, is formed through a surface breakup. The preparation of the nickel wire is also described in previous publication [13]. Briefly, the nickel wire with 0.4 mm diameter (TEMCO Inc.) is cut into 50 mm lengths. The cut wires are then cleaned by sonication in an acetone solution for 15 minutes, followed by sonication in distilled water. The wires are dried in the open air before inserted into a flame using substrate holder as shown in Figure 5.

Diffusion flame setup and synthesis

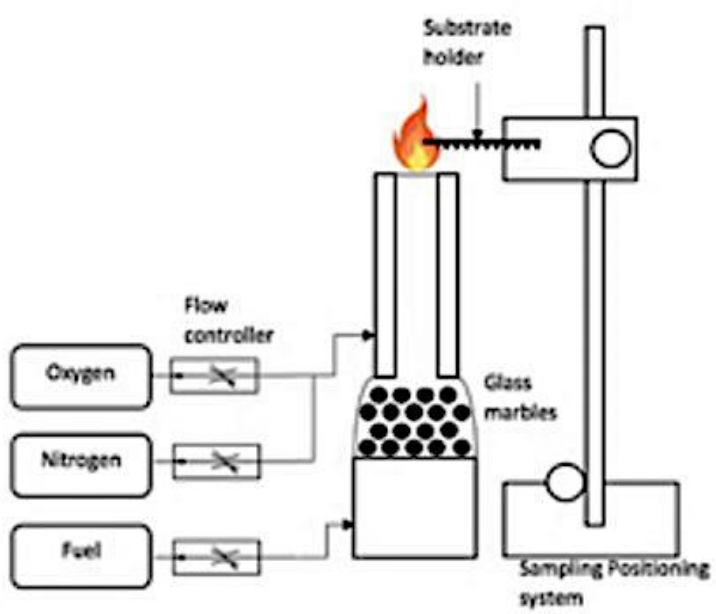

Figure 5: Laminar diffusion flame synthesis setup employing precision traversing arm with an accuracy of 1mm

Figure 5 shows the diffusion flame synthesis setup in which a laminar diffusion flame burner is utilized with methane gas that is set up through concentric fuel and oxidizer outlet tubes of a 17 mm and 26 mm diameter, respectively. The 99.995% methane gas was supplied through the central tube at a fixed rate of 0.4 slpm, controlled by the Omron^{TM} flow sensor. The concentric tube supplied the oxidizer gases consists of a mixture of 99.9% oxygen at a fixed rate of 0.7 slpm and 99.9% nitrogen at a fixed rate of 3.0 slpm, controlled by metering valves equipped with Honeywell^{TM} sensors. The flame is established with a global equivalence ratio of 1.16 and an oxygen concentration of 19%. The cleaned nickel wire was exposed to the flame using a traversing system which positioned the wire at desired location with an accuracy of 1mm. Analogous to the previous publication [13], the synthesis starts with nickel wire exposed to an open flame at a height-above-burner (HAB) of 4 mm up to 14 mm for 3 minutes. The methane diffusion flame was unable to form under the wire mesh below 4 mm HAB, whereas CNT was not synthesized on the nickel wire above 15 mm HAB. The whole synthesis was done within a burner enclosure at atmospheric pressure. In addition, an extractor fan was used to further minimize the surrounding air disturbance to the flame.

Premixed flame setup and synthesis

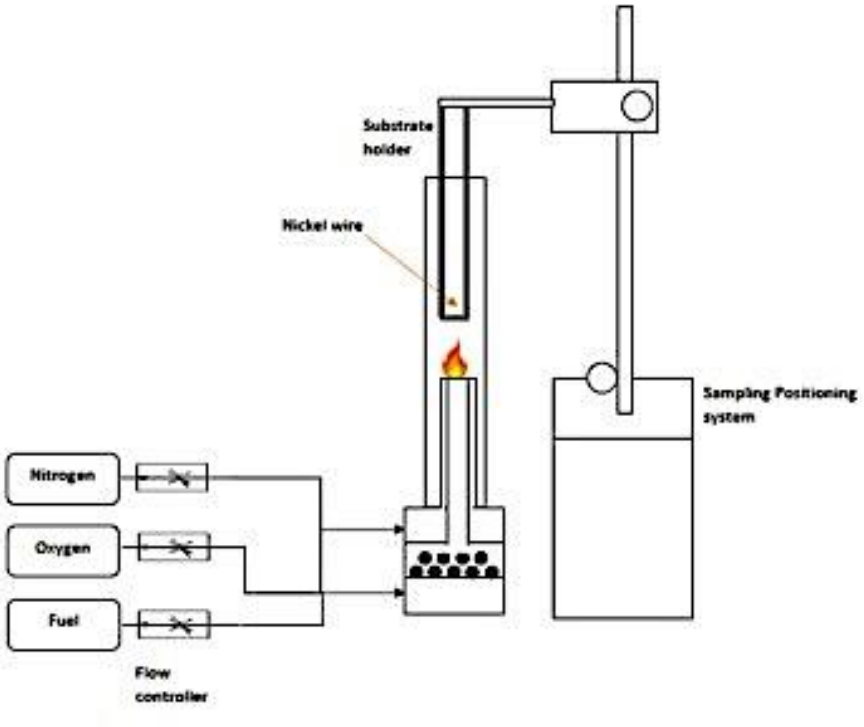

Figure 6: Schematic diagram of premixed flame synthesis setup with quartz tube and precision traversing arm. The one-dimensional flame is achieved with the utilization of sintered metal at the outlet of the burner.

Figure 6 shows the schematic diagram of the CNT synthesis setup using premixed burner with sintered metal at the outlet of the burner. The burner consists of a premixed chamber and concentric nozzle tube outlet for mixture and shield gas with 17 mm and 26 mm diameters, respectively. A quartz tube with an outer diameter of 50 mm is inserted into the burner nozzle. The positioning system with an accuracy of 0.5 mm is employed for the sampling method. The sample will be placed on top of a mesh wire coupled at the bottom of the sampling probe. The probe is inserted into the quartz tube vertically from

the top. The length of the insertion is adjusted to vary the HAB of the samples from 5-17 mm. Unless otherwise noted, the sampling time is fixed at 1 min for all runs.

The combustion of the premixed flame is done through a premixed of methane gas at 99.995% purity, oxygen gas at 99.9% purity, and nitrogen gas at 99.9% purity; all controlled with Kofloc flow controllers at 0.4 slpm, 0.445 slpm, and 0.8 slpm, respectively. The mixture produces a flat flame burned at a 1.8 equivalence ratio and 34% oxygen concentration. The flame was stabilized by flowing Nitrogen as shield gas at 6 slpm, removing the secondary flame simultaneously.

Flame and CNT Characterization

The flame temperature is measured using a type-B thermocouple with 0.5mm bead size (Omega Engineering) and traversing system with a sensitivity of 0.5 mm. The thermocouple is mounted at the end of solid arms, where the traversing system moves the thermocouple bead to a specific location within the flame. For accuracy, different location measurements were done by moving the arm in and out of the flame.

The grown CNT was characterized by Field Emission Scanning Electron Microscope (FESEM)(Zeiss Crossbeam 340) coupled with Energy Dispersive X-ray analysis (EDX) for morphology and elemental analysis. Raman spectroscopy analysis (HORIBA XploRA PLUS, 532 nm) was done to analyze the signature spectrum of the CNT grown.

Acknowledgments

This research was supported by the Ministry of Education (MOE) through the Fundamental Research Grant Scheme (FRGS/1/2020/TK0/UTM/02/54) with cost center number R.J130000.7851.5F377 and (FRGS/ 1/ 2019/ TK05/ UTM/02/8) with cost center

number R.J130000.7851.5F182. The research is also funded by Universiti Teknologi Malaysia (UTM) through UTM Fundamental Research (UTMFR: PY/2019/01657) grant with cost center number Q.J130000.2551.21H10.

References

[1] Sumio Iijima, “Helical microtubules of graphitic carbon,” *Nature*, vol. 354, no. 354, pp. 56–58, 1991.

[2] N. Gupta, S. M. Gupta, and S. K. Sharma, “Carbon nanotubes: synthesis, properties and engineering applications,” *Carbon Letters*, vol. 29, no. 5. Springer Singapore, pp. 419–447, 2019, doi: 10.1007/s42823-019-00068-2.

[3] S. Shahidi and B. Moazzenchi, “Carbon nanotube and its applications in textile industry – A review,” *J. Text. Inst.*, vol. 5000, pp. 1–14, 2018, doi: 10.1080/00405000.2018.1437114.

[4] A. Iqbal, A. Saeed, and A. Ul, “A review featuring the fundamentals and advancements of polymer / CNT nanocomposite application in aerospace industry,” *Polym. Bull.*, vol. 78, no. 1, pp. 539–557, 2021, doi: 10.1007/s00289-019-03096-0.

[5] M. Scarselli *et al.*, “Applications of three-dimensional carbon nanotube networks,” *Beilstein J. Nanotechnol.*, vol. 6, no. 1, pp. 792–798, 2015, doi: 10.3762/bjnano.6.82.

[6] X. Wang, A. Dong, Y. Hu, J. Qian, and S. Huang, “Recent Review on Using Metal-Organic Frameworks to Grow Carbon Nanotubes Xian,” *Chem. Commun.*, no. 56, pp. 10809–10823, 2020, doi: 10.1039/D0CC04015K.

[7] Y. Mo *et al.*, “Facile flame catalytic growth of carbon nanomaterials on the surface

of carbon nanotubes," *Appl. Surf. Sci.*, vol. 465, no. September 2018, pp. 23–30, 2019, doi: 10.1016/j.apsusc.2018.09.139.

[8] N. Hamzah, M. F. M. Yasin, M. Z. M. Yusop, A. Saat, and N. A. M. Subha, "Rapid Production of Carbon Nanotubes: A Review on Advancement in Growth Control and Morphology Manipulations of Flame Synthesis," *Mater. Chem. Ahemistry A*, 2017, doi: 10.1039/C7TA08668G.

[9] N. Hamzah *et al.*, "Effect of fuel and oxygen concentration toward catalyst encapsulation in water-assisted flame synthesis of carbon nanotubes," *Combust. Flame*, vol. 220, pp. 272–287, 2020, doi: 10.1016/j.combustflame.2020.07.007.

[10] C. Zhang *et al.*, "Synthesis of single-walled carbon nanotubes in rich hydrogen/air flames," *Mater. Chem. Phys.*, vol. 254, no. 6, p. 123479, 2020, doi: 10.1016/j.matchemphys.2020.123479.

[11] E. G. O. Casanova, A. T. Mandujano, and M. Rom, "Microscopy and Spectroscopy Characterization of Carbon Nanotubes Grown at Different Temperatures Using Cyclohexanol as Carbon Source," vol. 2019, 2019.

[12] C. Tung *et al.*, "Morphology and growth of carbon nanotubes catalytically synthesised by premixed hydrocarbon-rich flames Catalyst-supported," *Mater. Chem. Phys.*, vol. 197, pp. 246–255, 2017, doi: 10.1016/j.matchemphys.2017.05.036.

[13] N. Hamzah, M. F. M. Yasin, M. Z. M. Yusop, A. Saat, and N. A. M. Subha, "Diamond & Related Materials Growth region characterization of carbon nanotubes synthesis in heterogeneous fl ame environment with wire-based macro-image analysis," *Diam. Relat. Mater.*, vol. 99, no. May, p. 107500, 2019, doi:

10.1016/j.diamond.2019.107500.

[14] M. Notarianni, J. Liu, K. Vernon, and N. Motta, “Synthesis and applications of carbon nanomaterials for energy generation and storage,” *Beilstein J. Nanotechnol.*, vol. 7, pp. 149–196, 2016, doi: 10.3762/bjnano.7.17.

[15] J. Wu, K. Liang, C. Yang, J. Zhu, and D. Liu, “Synthesis of carbon nanotubes on metal mesh in inverse diffusion biofuel flames,” *Fullerenes Nanotub. Carbon Nanostructures*, vol. 27, no. 1, pp. 77–86, 2019, doi: 10.1080/1536383X.2018.1523149.

[16] N. Hamzah *et al.*, “Morphology and Growth Region Analysis of Carbon Nanotubes Growth in Water-Assisted Flame Synthesis,” *Combust. Sci. Technol.*, vol. 00, no. 00, pp. 1–18, 2021, doi: 10.1080/00102202.2021.1991332.

[17] F. Migliorini, S. De Iuliis, F. Cignoli, and G. Zizak, “How ‘flat’ is the rich premixed flame produced by your McKenna burner?,” *Combust. Flame*, vol. 153, no. 3, pp. 384–393, 2008, doi: 10.1016/j.combustflame.2008.01.007.

[18] W. Han, D. Chen, Q. Li, W. Liu, H. Chu, and X. Rui, “Ultrafast flame growth of carbon nanotubes for high-rate sodium storage,” *J. Power Sources*, vol. 439, no. July, p. 227072, 2019, doi: 10.1016/j.jpowsour.2019.227072.

[19] H. Chu, W. Han, F. Ren, L. Xiang, Y. Wei, and C. Zhang, “Flame Synthesis of Carbon Nanotubes on Different Substrates in Methane Diffusion Flames,” *ES Energy Environ.*, pp. 73–81, 2018, doi: 10.30919/esee8c165.

[20] C. M. Orofeo, H. Ago, N. Yoshihara, and M. Tsuji, “Micro Review Methods to Horizontally Align Single-Walled Carbon Nanotubes on Amorphous Substrate,” *Micro Rev.*, vol. 2, pp. 36–40, 2010.

[21] R. T. K. Baker, M. A. Barber, P. S. Harris, F. S. Feates, and R. J. Waite, “Nucleation and Growth of Carbon Deposits from the Nickel Catalyzed Decomposition of Acetylene,” vol. 62, pp. 51–62, 1972.

[22] R. T. K. Baker, “Catalytic Growth of carbon filament,” *Carbon N. Y.*, vol. 27, no. 3, pp. 315–323, 1989, doi: 10.1016/0008-6223(89)90062-6.

[23] M. V Kharlamova, “Investigation of growth dynamics of carbon nanotubes,” *Beilstein J. Nanotechnol.*, vol. 8, pp. 826–856, 2017, doi: 10.3762/bjnano.8.85.

[24] J. P. Gore and A. Sane, “Flame Synthesis of Carbon Nanotubes,” in *Carbon Nanotubes- Synthesis, Characterization, Applications*, InTech, 2011, pp. 55–61.

[25] J. Geng *et al.*, “Nickel formate route to the growth of carbon nanotubes,” *J. Phys. Chem. B*, vol. 108, no. 48, pp. 18446–18450, 2004, doi: 10.1021/jp047898p.

[26] A. T. Delariva, T. W. Hansen, S. R. Challa, and A. K. Datye, “In situ Transmission Electron Microscopy of catalyst sintering,” *J. Catal.*, vol. 308, pp. 291–305, 2013, doi: 10.1016/j.jcat.2013.08.018.

[27] F. Yang, M. Wang, D. Zhang, J. Yang, M. Zheng, and Y. Li, “Chirality Pure Carbon Nanotubes: Growth, Sorting, and Characterization,” *Chem. Rev.*, vol. 120, no. 5, pp. 2693–2758, 2020, doi: 10.1021/acs.chemrev.9b00835.

[28] J. H. Lehman, M. Terrones, E. Mansfield, K. E. Hurst, and V. Meunier, “Evaluating the characteristics of multiwall carbon nanotubes,” *Carbon N. Y.*, vol. 49, no. 8, pp. 2581–2602, 2011, doi: 10.1016/j.carbon.2011.03.028.

[29] R. A. DiLeo, B. J. Landi, and R. P. Raffaelle, “Purity assessment of multiwalled carbon nanotubes by Raman spectroscopy,” *J. Appl. Phys.*, vol. 101, no. 6, pp. 1–5, 2007, doi: 10.1063/1.2712152.

The Control on Morphology and Crystallinity of CNT in Flame Synthesis with One-Dimensional Reaction Zone

DIFFUSION FLAME

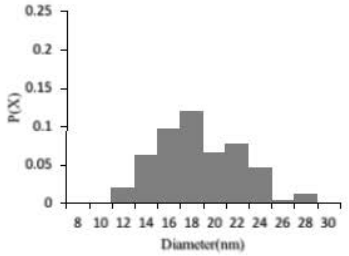

(a) HAB 6 mm

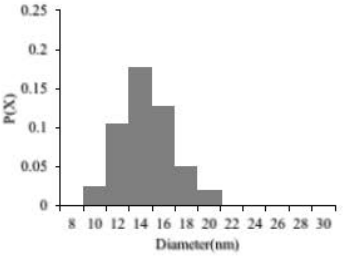

(b) HAB 8 mm

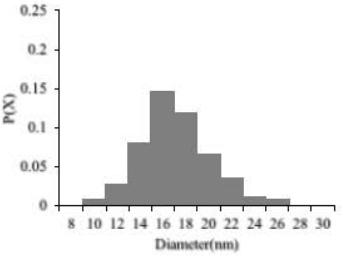

(c) HAB 10 mm

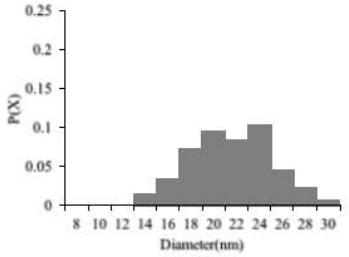

(d) HAB 12 mm

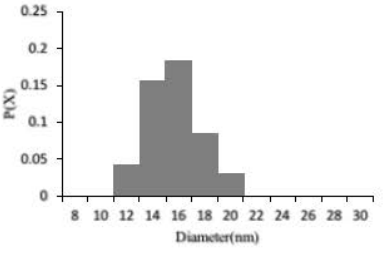

(e) HAB 16 mm

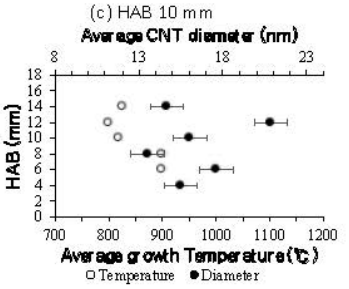

(f) Summary

PREMIXED FLAME

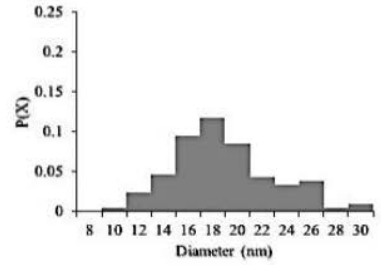

(a) HAB 5 mm

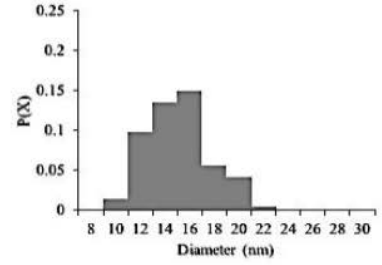

(b) HAB 10 mm

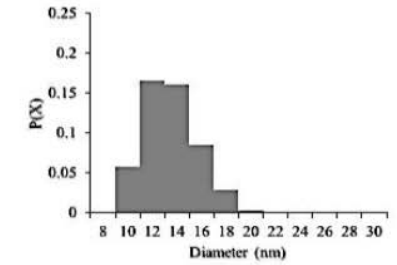

(c) HAB 11 mm

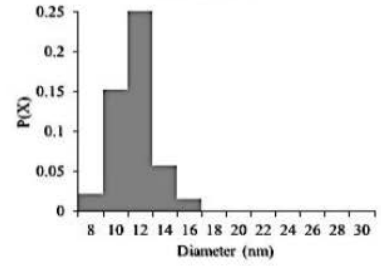

(d) HAB 15 mm

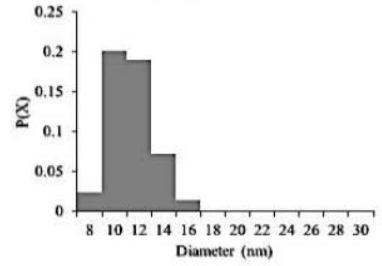

(e) HAB 17 mm

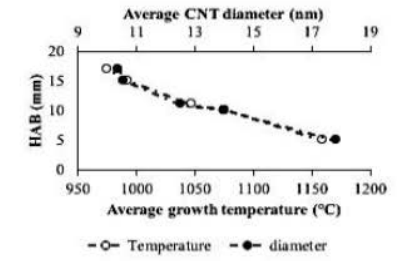

(f) Summary